Magnetic properties of zinc ferrite nanoparticles synthesized by hydrolysis in a polyol medium



2006 J. Phys.: Condens. Matter 18 9055

(http://iopscience.iop.org/0953-8984/18/39/032)

INSTITUTE OF PHYSICS PUBLISHING JOURNAL OF PHYSICS: CONDENSED MATTER

J. Phys.: Condens. Matter **18** (2006) 9055–9069 doi:10.1088/0953-8984/18/39/032

# Magnetic properties of zinc ferrite nanoparticles synthesized by hydrolysis in a polyol medium

**Souad Ammar[1,6], Noureddine Jouini[1,2], Fernand Fiévet[1], Zyed Beji[1,3], Leila Smiri[3], Philippe Moliné[4], Michel Danot[4] and Jean-Marc Grenèche[5]**

[1] ITODYS, UMR-CNRS 7086, Université Paris 7, 75251 Paris, France
[2] LPMTM, UPR-CNRS 9001, Institut Galilée, 93430 Villetaneuse, France
[3] LSSMI, UR-99/1230, Faculté des Sciences de Bizerte, 7021 Zarzouna, Tunisia
[4] Institut Jean Rouxel des Matériaux, 44072 Nantes, France
[5] LPEC, UMR-CNRS 6087, Université du Maine, 72085 Le Mans, France

E-mail: ammarmer@ccr.jussieu.fr

Received 27 April 2006, in final form 25 July 2006
Published 15 September 2006
Online at stacks.iop.org/JPhysCM/18/9055

**Abstract**

Highly crystalline, nanometre sized $ZnFe_2O_4$ particles with different diameters, 6.6 and 14.8 nm, were prepared by forced hydrolysis in a polyol medium. The DC magnetic properties exhibit a strong dependence on the particle size as a result of the unusual cation distribution. They clearly establish their superparamagnetic character at room temperature and the occurrence of ferrimagnetic or ferromagnetic ordering at low temperature. The magnetization is found to increase with grain size reduction. The $^{57}$Fe Mössbauer spectra were recorded at 300 and 4.5 K. There is no evidence for the presence of the $Fe^{2+}$ charge state, confirming the perfect stoichiometry of the two samples. At 300 K, the Mössbauer spectra consist of doublets due to the superparamagnetic behaviour whereas at 4.5 K they reveal a magnetically blocked state. Mössbauer spectra at 10 K in an external 6 T magnetic field applied parallel to the direction of the gamma rays clearly show a close to collinear Néel-like ferrimagnetic ordering for the 6.6 nm particles and a canted Yafet–Kittel-like ferrimagnetic ordering for the 14.8 nm ones.

(Some figures in this article are in colour only in the electronic version)

## 1. Introduction

Ferrites, $MFe_2O_4$, have been used for a long time in a variety of magnetic materials including information storage media. The magnetic properties of ferrites depend on the cation distribution in the spinel lattice. Thermodynamically, the degree of structure inversion in the spinel lattice,

[6] Corresponding address: Université Paris 7 (case 7090), 2 Place Jussieu 75251 Paris cedex 05, France.

  

defined by the ratio of the number of $Fe^{3+}$ ions in tetrahedral sites to the total number of $Fe^{3+}$ ions, depends on the ionic radius, the configuration of the cations and their relative stabilization energies in the tetrahedral and octahedral electrostatic fields. However, this parameter can be affected by the conditions of sample preparation, and a metastable local structure can be observed. This is particularly the case for zinc ferrite.

Stoichiometric bulk $ZnFe_2O_4$ prepared by the classical ceramic route exhibits a normal spinel structure where $Zn^{2+}$ and $Fe^{3+}$ ions occupy the tetrahedral (A) and the octahedral (B) spinel sites, respectively [1]. It displays a long-range antiferromagnetic ordering below 10 K [2] with zero magnetization at low temperature. Indeed, the magnetic ordering in ferrites is driven by the A–A, B–B and A–B interactions. The intra-site interaction of the magnetic moment of the cations on the A or B sites is much weaker than the A–B inter-site one. If the tetrahedral sites are exclusively occupied by non-magnetic ions, magnetic interaction occurs only between $Fe^{3+}$ ions in the octahedral sites, and the weak negative B–B interaction leads to an antiferromagnetic long-range order.

Stoichiometric $ZnFe_2O_4$ nanoparticles can be prepared by a *chimie douce* route, involving aqueous co-precipitation [3–6], low temperature supercritical sol–gel drying [7, 8], microemulsion [9], hydrothermal synthesis [10, 11] while nanostructured powders are obtained using high energy ball milling [12, 13] and mechanochemistry [42, 43]. Both systems exhibit a partially inverted spinel structure where a non-zero number of $Fe^{3+}$ ions occupy A sites, as observed by EXAFS [14, 15], neutron diffraction [16, 17] and/or Mössbauer spectrometry [13, 18, 19]. They display non-zero magnetization even at low temperature. Indeed, when the concentration of magnetic ions in A sites is below the percolation limit 0.33, which corresponds to a structure inversion of 16.5% [20], magnetic frustration resulting from the competition between A–B and B–B interactions and the magnetic disorder on B sites gives rise to spin glass-like behaviour. Magnetic clusters are formed due to the presence of short-range magnetic ordering and freeze in random directions below the spin freezing temperature. When this concentration is higher, and according to the Yafet–Kittel model [35], canting in both A and B sublattices is observed and the spinel adopts a planar canted ferrimagnetic long-range structure, with magnetic ordering temperatures much higher than the classical Néel temperature of normal $ZnFe_2O_4$, which can be as high as 460 K [21].

In this paper, we report the magnetic properties of two samples of $ZnFe_2O_4$ nanoparticles. These particles were prepared by forced hydrolysis in polyol [14]. They are almost equiaxed with mean diameters of 6.6 and 14.8 nm, with a standard deviation less than 10%. They have a degree of structure inversion of 25 and 15% respectively [14], namely higher and closer than the percolation limit, respectively. They are highly crystalline, as are all nanocrystallized oxides prepared by this method ($CoFe_2O_4$ [23], $MnFe_2O_4$ [24] or $NiFe_2O_4$ [25], . . .), and can then be considered as quasi-ideal materials for studying the intrinsic properties of partially inverted $ZnFe_2O_4$ spinel without the usual problems related to the reduction of the particle size, such as an important spin glass contribution due to the disorder of the magnetic moment orientation on the surface of the particles and/or a non-negligible canting appearance due to the break-up of magnetic exchange paths in the core of the particles related to their poor crystallinity [22].

Our results confirm without any ambiguity that polyol-prepared stoichiometric $ZnFe_2O_4$ nanocrystals exhibit ferrimagnetic ordering due to the change in cation distribution when the particle size is reduced. We have found, by DC SQUID measurements and in-field $^{57}Fe$ Mössbauer spectrometry, that a high degree of structure inversion, typically 25%, leads to a close to collinear Néel-like ferrimagnetic structure while a low one, typically 15–18%, leads to a canted Yafet–Kittel-like one.

## 2. Experimental details

The 6.6 and 14.8 nm $ZnFe_2O_4$ particles were prepared according to the procedure described in [14]. The XRD patterns were recorded using a powder diffractometer with Fe K$\alpha$ radiation. The size of the particles was determined by TEM images and the degree of cationic inversion was estimated by EXAFS and XMCD measurements and was found to be about 25% and 15%, respectively.

The magnetic susceptibility and hysteresis loop measurements were performed on a SQUID magnetometer. The DC magnetic susceptibility $\chi(T)$ was measured in ZFC (zero-field cooling) and FC (field cooling) modes at 4.5–320 K with a magnetic field, $H$, of 50, 500 and 1000 Oe. The ZFC magnetization curves $M(H)$ were obtained at $H = -50$ to 50 kOe, at different temperatures.

The $^{57}$Fe Mössbauer spectra were recorded in a transmission geometry using a $^{57}$Co/Rh $\gamma$-ray source. Spectra were obtained at 300 and 4.2 K in zero magnetic field and at 10 K in a 6 T field oriented parallel to the $\gamma$-beam. Mössbauer spectra were analysed by a least-squares fitting method using Lorentzian functions. The isomer shifts ($\delta$) were referred to that of $\alpha$-Fe at 300 K.

## 3. Results and discussion

### *3.1. Phase analysis*

Figure 1(A) shows the XRD patterns of the 6.6 and 14.8 nm $ZnFe_2O_4$ particles prepared by forced hydrolysis in polyol [14]. All the diffraction peaks are attributable to the spinel phase. The lattice parameters are obtained by a least-squares refinement using the Ufit program [36] and are found to be comparable to that of bulk $ZnFe_2O_4$, $a = 8.44$ Å (JDPDS 22-1012). The particles are single crystals since their diameter determined by TEM measurements agrees fairly well with the crystal size inferred from XRD line broadening using the Scherrer formula [14]. They appear in TEM images (figure 1(B)) with a quasi-spherical shape and a uniform size (the standard deviation of the particle size is found to be 0.2 and 0.8 nm for the smaller and the larger particles, respectively) and relatively agglomerated in one case and not in the other. Moreover, a zoom on a representative particle (inset of figure 1(B)) confirms the high crystalline quality of the prepared materials. There are no defects such as dislocations and stacking faults.

### *3.2. Magnetic measurements*

The ZFC and FC magnetic susceptibility, $\chi$, measurements conducted on the two kinds of particles, 6.6 and 14.8 nm, at 50, 500 and 1000 Oe, are presented in figure 2. A net irreversibility between the curves measured in the FC and ZFC modes is systematically observed in DC susceptibility measurements whatever the size of the particles and the applied magnetic field: the ZFC $\chi(T)$ curve shows a cusp decreasing rapidly to zero at lower temperature, while FC $\chi(T)$ departs from ZFC one as the temperature decreases, from the cusp temperature to 4.5 K. In all the cases, the ZFC and FC curves are perfectly superimposed only at high temperature. At $H = 50$ Oe, the ZFC $\chi(T)$ cusp is around 89 K for the 6.6 nm sized particles and 20 K for the 14.8 nm sized ones. The nanoparticles can therefore be considered as magnetic single domains. A good estimation of the blocking temperature, $T_B$, value is given by the temperature position of the maximum of the ZFC $\chi(T)$ curve, in agreement with the usual procedure [19, 26]. It is found to be around 89 K (at 50 Oe) for 6.6 nm particles and of 20 K (at 50 Oe) for the 14.8 nm one. This blocking temperature decreases when the applied magnetic

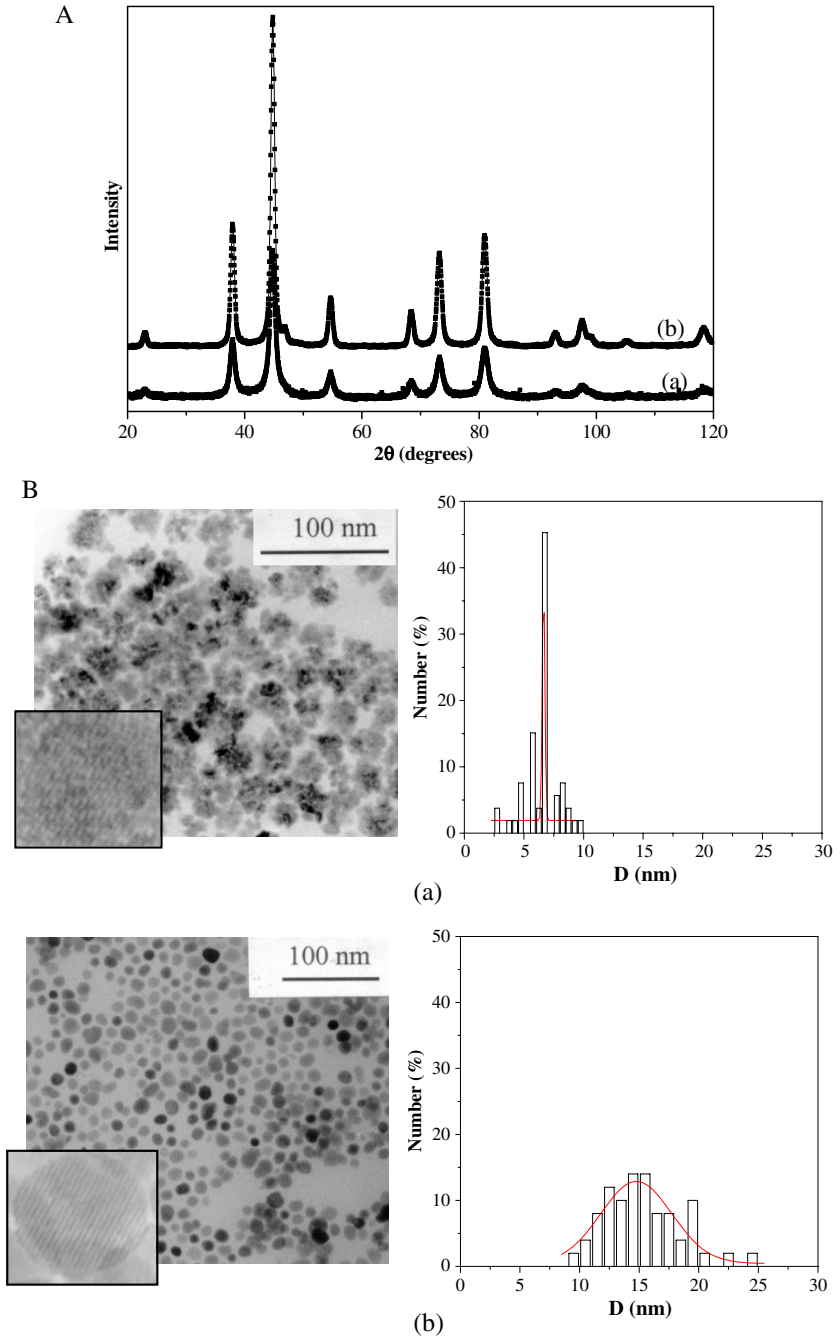


**Figure 1.** (A) XRD pattern of (a) 6.6 nm and (b) 14.8 nm $ZnFe_2O_4$ particles. (B) TEM image of a collection of particles and the histogram of the particle size of (a) 6.6 nm and (b) 14.8 nm $ZnFe_2O_4$ particles. In each case, the HRTEM micrograph of one representative particle is given in the inset.

field increases, as expected for a superparamagnet [38]. For more clarity all the magnetic characteristics of the two samples are summarized in table 1.

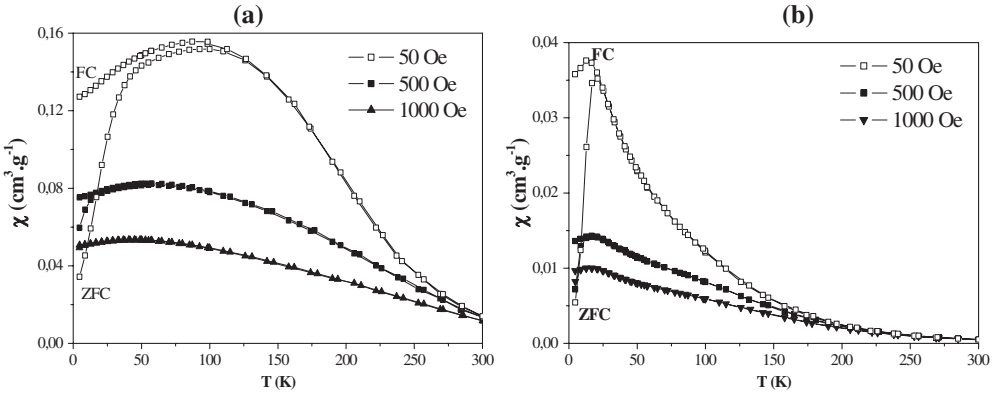


**Figure 2.** ZFC and FC susceptibility measured at 50, 500 and 1000 0e, at 4.5–320 K for (a) 6.6 nm and (b) 14.8 nm $ZnFe_2O_4$ particles.

**Table 1.** Magnetic characteristics of 6.6 and 14.8 nm $ZnFe_2O_4$ particles.

| Size (nm) | $T_B$ (K) | $M_{rem}/M_{sat}$ | $H_c$ (kOe) | $M_{(50\ kOe)}$ (emu $g^{-1}$) |
|---|---|---|---|---|
| 6.6 | 89 (50 Oe) | 0.20 (5 K) | 0.2 (5 K) | 76.8 (5 K) |
| | 59 (500 Oe) | | | 37.0 (300 K) |
| | 44 (1000 Oe) | | | |
| 14.8 | 20 (50 Oe) | 0.10 (5 K) | 0.4 (5 K) | 42.5 (5 K) |
| | 18 (200 Oe) | | | 12.0 (300 K) |
| | 16 (500 Oe) | | | |
| | 13 (1000 Oe) | | | |

It must be noted that the blocking temperature is less well defined for the smaller particles than for the larger ones. Indeed, the temperature dependence of the magnetic susceptibility differs significantly from one sample to another when they are cooled further. Around $T_B$, whereas the ZFC $\chi(T)$ curve of the 6.6 nm particles displays a cusp almost truncated to reach nearly a plateau, despite their monodisperse character (see figure 1(B)), the ZFC $\chi(T)$ curve of the 14.8 nm ones exhibits a net maximum. Moreover, the FC $\chi(T)$ curve, when it departs from the ZFC one, decreases slightly with decreasing temperature, for the two samples, while it is expected to show, in superparamagnetic materials, either an increase or a plateau as the temperature decreases below $T_B$. This decrease is more pronounced for the smaller particles than for the larger ones. To the best of our knowledge, such features have seldom been observed for superparamagnetic monodisperse particles. They were reported for non-stoichiometric zinc ferrite prepared by the microemulsion route, and attributed by the authors to the intrinsic ferromagnetic structure of the particles, without excluding some dipolar contribution [9], and for almost stoichiometric $ZnFe_2O_4$ nanoparticles prepared by co-precipitation [26], and attributed by the authors to the combination of the blocking of the magnetic moment of each particle and the magnetic interaction between the particles. On the other hand, some authors, like Makhlouf *et al* [39] and Chantrell *et al* [40], observed that the FC $\chi(T)$ curve for a non-interacting superparamagnet continues to rise approximately as $1/T$ with decrease in temperature, below the blocking temperature, and proposed that a deviation from this variation must be due to interparticle interactions. These reports suggest that, for our

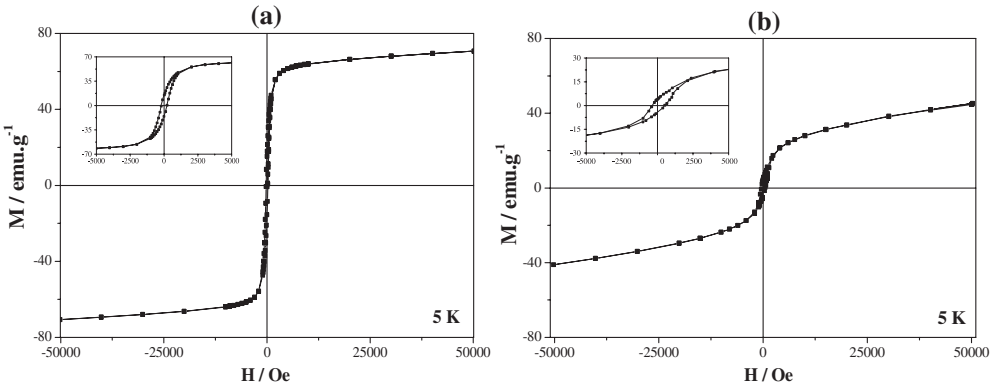


**Figure 3.** ZFC magnetization versus magnetic field measured at 5 K for (a) 6.6 nm and (b) 14.8 nm $ZnFe_2O_4$ particles. A zoom for low field in given in the inset.

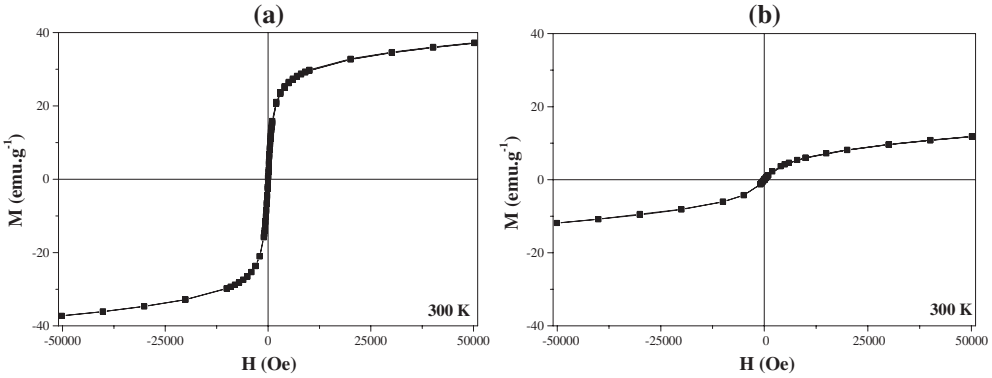


**Figure 4.** ZFC magnetization versus magnetic field measured at 300 K for (a) 6.6 nm and (b) 14.8 nm $ZnFe_2O_4$ particles.

compact $ZnFe_2O_4$ powders, and particularly in the case of the smaller particles, dipole–dipole interactions are present and must be responsible for the unusual ZFC and FC $\chi(T)$ behaviour observed around and below $T_B$, these interactions being greater for the smaller particles. This hypothesis is somewhat confirmed in regard to the collected TEM images where the smaller particles appear clearly agglomerated and the larger do not.

Additional experiments were run on our samples in order to characterize their magnetic properties. The variations of the ZFC isothermal magnetization with the applied magnetic field at 5 and 300 K are given in figures 3 and 4, respectively. Hysteresis loops were observed at low temperature ($T < T_B$) with both remanence and coercivity which increase when the temperature decreases. At 5 K, the observed values of the squareness ratio and coercivity are 0.20 and 0.15 kOe, respectively, for the smaller particles and 0.10 and 0.41, respectively, for the larger ones. The observation of hysteresis loops below the blocking temperature is not consistent with the antiferromagnetic ordering reported for bulk $ZnFe_2O_4$ and suggests clearly the occurrence of a ferrimagnetic or a ferromagnetic ordering in these nanocrystals. When the temperature is increased, the magnetization value decreases owing to thermal fluctuations, and the hysteresis feature disappears, in agreement with the superparamagnetic character of

**Table 2.** Comparison of the degree of structure inversion, the blocking temperature, $T_B$, and the saturation magnetization of $ZnFe_2O_4$ nanoparticles obtained by different synthesis methods.

| Reference | Synthesis method | Size (nm) | $\delta$ (%) | Method of determination of the local structure | $M_{sat}$ (emu $g^{-1}$) |
|---|---|---|---|---|---|
| This work, [14] | Polyol method | 6.6<br>14.8 | 25<br>18 | In 6 T field—Mössbauer spectroscopy at 10 K | 78.0 (5 K)<br>53.9 (5 K) |
| [8] | Supercritical sol–gel + drying at 513 K | 8.1 | 22 | Rietveld refinement on x-ray diffraction | 22 (5 K) |
| | Supercritical sol–gel + drying at 513 K + ball milling for 10 h | 10.3 | 10.3 | Rietveld refinement on x-ray diffraction | 73 (10 K) |
| [33] | Hydrothermal in supercritical methanol | 5–20 | 0 | Mössbauer spectroscopy at RT | 38 (4.2 K) |
| [34] | Hydrothermal in ammonia solution | 300 | $\neq 0$ | Cationic inversion suspected | 61.2 (80 K) |
| [17] | Ball milling | 36 | 7 | Rietveld refinement on neutron diffraction | 20.7 (4.2 K) |
| | Ball milling + calcination at 773 K | 50 | 16 | Rietveld refinement on neutron diffraction) | 40.3 (4.2 K) |
| [13] | Ball milling | 11 | 36 | In 6 T field—Mössbauer spectroscopy at 10 K | 10 (300 K) |
| | | 14 | 24 | In 6 T field—Mössbauer spectroscopy at 10 K | 7.5 (300 K) |
| [21] | Ball milling | 9 | 43 | Rietveld refinement on neutron diffraction | 58 (5 K) |
| [3, 15] | Co-precipitation at 373 K | 5.5 | $\neq 0$ | EXAFS analysis at Zn K edge | 35 (4.2 K) |
| | Co-precipitation at 373 K + calcination at 973 K | 96.0 | 11 | In 6 T field—Mössbauer spectroscopy at 10 K | Not given |
| [16] | Co-precipitation at 373 K | 5.5 | $\neq 0$ | Cationic inversion suspected | 46.9 (5 K) |
| | Co-precipitation at 373 K + calcination at 773 K | 29 | 7 | Rietveld refinement on neutron diffraction | 26.4 (5 K) |

the particles. The saturation magnetization, $M_{sat}$, at 5 K, is determined by extrapolating the $M$ versus $1/H$ curve to $1/H = 0$. It is found to be very close to that measured at 50 kOe for the 6.6 nm particles (78.0 instead 76.8 emu $g^{-1}$), and quite different for the 14.8 nm ones (53.9 instead 42.5 emu $g^{-1}$). The particular lack of saturation of this sample will be discussed later. It must be pointed out that the saturation magnetization measured for the 6.6 nm particles is the highest value ever observed for almost stoichiometric zinc ferrite nanoparticles, if we except the particles prepared by the microemulsion route which exhibit a significant non-stoichiometry [9] and the nanostructured powders prepared by the ball milling route which exhibit a large degree of cationic inversion [8]. Table 2 compares the main magnetic characteristics of the polyol-prepared nanoparticles with those of similar ones prepared by other methods. To our knowledge, the improved magnetic properties measured here are essentially due to a combination of cationic inversion and high crystalline quality related to the specific thermal growth conditions in polyol. It is thus possible to estimate the total saturation of the bulk counterpart of these nanoparticles, assuming the same degree of cationic inversion (25%), and to compare it with the experimental nanocrystal value, with that measured at 5 K. It is calculated using the classical collinear ferrimagnetic Néel model

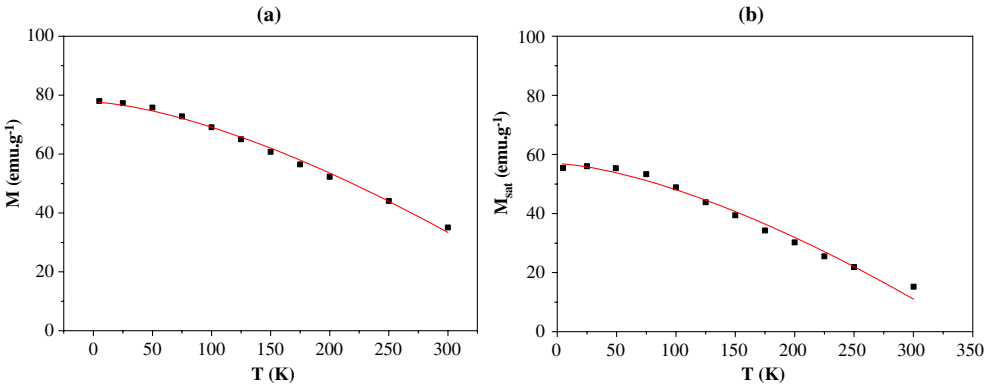


**Figure 5.** Thermal variation of the magnetization at 50 kOe of (a) 6.6 nm and (b) 14.8 nm $ZnFe_2O_4$ particles. The line corresponds to the magnon-type Bloch law fit.

corrected for randomly incomplete linkages, due to the presence of diamagnetic cations in the superexchange interaction, according to Gilleo's equation [29]:

$$M_s = 2.\mu(\mathrm{Fe}_B^{3+}) \times [1 - k_o][1 - E_o(k_t)] - \mu(\mathrm{Fe}_A^{3+}) \times [1 - k_t][1 - E_t(k_o)] \tag{1}$$

where $\mu(\mathrm{Fe}_B^{3+})$ and $\mu(\mathrm{Fe}_A^{3+})$ are the magnetic moments of $Fe^{3+}$ ions in B and A sites, respectively; $k_o = 0.25, k_t = 0.50, E_o(k_t) = 0.10937$ and $E_t(k_o) = 2.2 \times 10^{-6}$ are constants related to the degree of cationic inversion. $M_s$ is found to be 95 emu $g^{-1}$ (instead of 115 emu $g^{-1}$ without the statistical correction), slightly higher than that measured for the nanocrystals (78 emu $g^{-1}$). The difference between the two values can be explained by the non-collinear magnetic structure in the nanoparticles, according to the expected Yafet–Kittel model, and/or a surface magnetic disorder induced by the lack symmetry. Neglecting the effect of the first canting origin, since the magnetization seems to reach saturation at $T < T_B$ for this sample, $M$ versus $H$ has an almost zero slope at higher $H$ (figure 3). The effect of the second one, namely the existence of a magnetically dead surface layer in the particles, seems to be relatively small but sufficient to slightly reduce the magnetization of the particles. It is possible to estimate the thickness of this layer using the equation of Zheng *et al* [37]:

$$M_{sat} = M_s(1 - 6t/D) \tag{2}$$

where $D$ is the diameter of the particles, as observed by microscopy, $t$ the thickness of the surface layer and $M_{sat}$ and $M_s$, the total saturation of the whole particle and of its bulk counterpart, respectively. $M_{sat}$ is deduced from the experimental magnetic data (78 emu $g^{-1}$) and $M_s$ was estimated from equation (1) (95 emu $g^{-1}$). The ratio $t/D$ is found to be very small, about 3%, and confirms that the magnetically dead shell is confined to a very thin surface layer.

The thermal variation of the saturation magnetization of the 6.6 nm (figure 5(a)) and 14.8 nm (figure 5(b)) particles is also examined. It is found to follow a magnon-type Bloch law of ferrimagnets or ferromagnets [27]. The plot of $M_{sat}$ versus $T$ is correctly fitted using the Bloch equation

$$M_{sat}(T) = M_{sat}(0)\{1 - B(T)^b\} \tag{3}$$

where $M_{sat}(0)$, $B$ and $b$ correspond to the 0 K saturation magnetization, the Bloch constant and the Bloch exponent, respectively. The values of these parameters for the two specimens were obtained by fitting the measured data to equation (3):

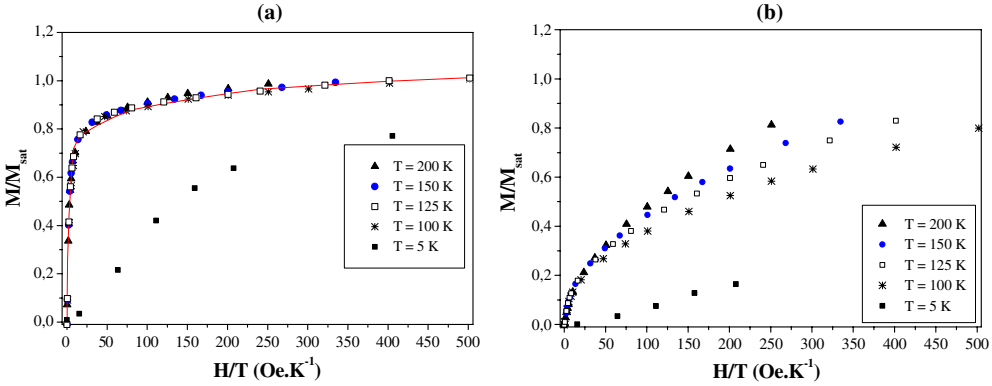


**Figure 6.** $M/M_{\mathrm{sat}}$ versus $H/T$, as measured at $T = 200$, 150, 125, 100 and 5 K for (a) 6.6 nm and (b) 14.8 nm particles. The solid line is the fit to equation (4).

(i) $b = 1.45$ and 1.55 for the smaller and larger particles, respectively, close to the value of bulk ferromagnetic or ferrimagnetic materials ($b = 1.5$ [27]) and slightly smaller than that usually reported for nanocrystalline ($b > 1.5$ [28]).

(ii) $B = 1.459 \times 10^{-4}\ K^{-b}$ and $1.176 \times 10^{-4}\ K^{-b}$ for the smaller and larger particles, respectively.

(iii) $M_{\mathrm{sat}}(0) = 79$ and 56 emu $\mathrm{g}^{-1}$, in agreement with the experimental value measured at 5 K on the 6.6 and 14.8 nm particles, respectively.

Several works reported a dependence of $b$ on the particle size in nanomagnets, ferrimagnetic or ferromagnets. It is found, for instance, in the range 1.6–1.8 for $MnFe_2O_4$ particles of 5–15 nm in size [28a], close to 1.9 [28b] and 1.66 [28c] for Fe–C and $La_{0.8}Sr_{0.2}MnO_{3-\delta}$ particles with a diameter of 3.1 and 8 nm, respectively. This deviation of $b$ from 1.5 is usually associated with the structural disorder increase with particle size reduction. In the case of the polyol-made particles, the great closeness between the fitted $b$ value and the expected 1.5 one can be related to their high crystalline quality. The same works underlined the dependence of the $B$ value with the size of the particle. It is usually found greater in nanoparticles than in bulk, increasing when the size decreases. Some authors attributed this feature to an increased interaction among the neighbouring spins [28c]. In the particular case of spinel ferrite materials it can be suspected to be due to a significant structural deviation from the thermodynamically stable one in terms of cation distribution. The 6.6 nm sized $ZnFe_2O_4$ particles exhibit the lower diameter, the higher degree of cationic inversion and then the higher $B$ value.

Moreover, the variation of the magnetization of the 6.6 nm particles as a function of $H/T$ follows a Langevin-type law (figure 6(a)) at $T > T_{\mathrm{B}}$, while it does not for the 14.8 nm ones (figure 6(b)). Indeed, for the smaller particles, the plot of $M(T)/M_{\mathrm{sat}}$ versus $H/T$ for $T = 100$, 125, 150 and 200 K, shown in figure 6(a), merges into a single curve, signifying superparamagnetism, whereas a similar analysis of the data at 5 K reveals a large departure from a Langevin-type law fit, as expected for $T < T_{\mathrm{B}}$. The refinement is performed using the equation

$$M(T) = M_{\mathrm{sat}}\{\coth(\mu H/kT) - (kT/\mu H)\} + \chi_a H \tag{4}$$

where $\mu$ is the magnetic moment/particle, $k$ the Boltzmann constant, $M(T)$ the magnetization of particles for a given temperature $T$, $M_{\mathrm{sat}}$ the total saturation of the overall particle, and $\chi_a$ the

high field susceptibility [30] which corresponds to a small correction to the classical Langevin equation [41]. The magnitude of $\mu$ is determined from the equation

$$\mu = M_s \rho V \tag{5}$$

where $\rho$ and $V$ are the density and volume of the particle, respectively. Assuming a spherical particle with diameter $D = 6.6$ nm [14], $\rho = 5.10$ g cm$^{-3}$ for $ZnFe_2O_4$, the fit yields $M_s = 95(4)$ emu g$^{-1}$, in agreement with the value estimated from equation (1), and $\chi_a = 9.3(0.5) \times 10^{-7}$ cm$^3$ g$^{-1}$. These results show, once again, that these polyol-made particles can be considered as almost perfectly magnetically ordered single-domain ones without significant surface and/or core canting.

The fact that the $M(T)/M_{sat}$ versus $H/T$ curves do not coalesce in figure 6(b), for the larger particles is, to our understanding, more probably due to the canting effects than to the dipolar interactions between particles. Indeed, the comparison of the TEM micrograph, on one hand, and the FC and ZFC $\chi(T)$ variation, on the other hand, for the 6.6 and 14.8 nm sized particles, shows that these interactions exist but are stronger in the smaller than in the larger particles. However, in the 6.6 nm particles the $M/M_{sat}$ $(H/T)$ curves coalesce.

It appears clearly that the magnetic characteristics of our materials completely differ from those of bulk $ZnFe_2O_4$ but are also different from one sample to another according to their degree of cationic inversion. We expected to observe in both samples canted Yafet–Kittel-like ordering below the blocking temperature, characterized by an important lack of saturation of the magnetization even at high magnetic field. Surprisingly, we observe this only for the larger particles, since for the smaller ones the magnetization, $M$, is close to saturation at 50 kOe. Usually, the lack of saturation, at $T < T_B$, of the magnetization versus $H$, in superparamagnets is related to a canting in the magnetic structure as a consequence of: (i) finite size scaling which leads to a non-collinearity of magnetic moments on their surface due to broken exchange bonds at the external layer of the particles (the surface spin having nearest neighbours on one side, none on the other side); (ii) poor crystallinity accompanied with great structural disorder which leads to non-collinearity of magnetic moments in their core due to break-up of magnetic exchange paths and (iii) more specifically, in the case of $ZnFe_2O_4$ nanocrystals, non-equilibrium distribution of the cations amongst the interstitial spinel sites which leads to a non-collinear arrangement of the magnetic moments in A and B sites resulting from competing antiferromagnetic interactions and leading to the well known canted Yafet–Kittel-like ferrimagnetic structure. In the present case, the local spin canting is only clearly apparent for the larger particles which have the lower surface to volume ratio, suggesting that the surface effects are almost negligible. Moreover, the high crystallinity, as already established for both, whatever the particle size, 6.6 or 14.8 nm [14], excluding any structural disorder contribution in the canting appearance of the $M$ versus $H$ curves, permits us to consider both kinds of particles as almost perfectly magnetically ordered single domains without significant surface and/or core canting, and then only the main difference in their degree of structure inversion should be considered to explain their magnetic behaviour difference. Indeed, the 6.6 nm particles exhibit a higher degree of cationic inversion (25%) than the 14.8 nm ones (15%). They correspond to the $(Fe_{0.5}Zn_{0.5})[Fe_{1.5}Zn_{0.5}]O_4$ formula, where the round and square brackets represent A and B spinel sites, respectively, and where the concentration of magnetic ions in the A sites, 0.50, is clearly higher than the percolation limits, 0.33. This suggests that, in the particular case of polyol-prepared 6.6 nm particles, the canting does not occur or at least can be neglected. A close to collinear Néel-like ordering takes place between the magnetic moments occupying the A and B sites, in agreement with the observed Bloch-like $M_{sat}(T)$ and the Langevin-like $M(H/T)$ behaviours.

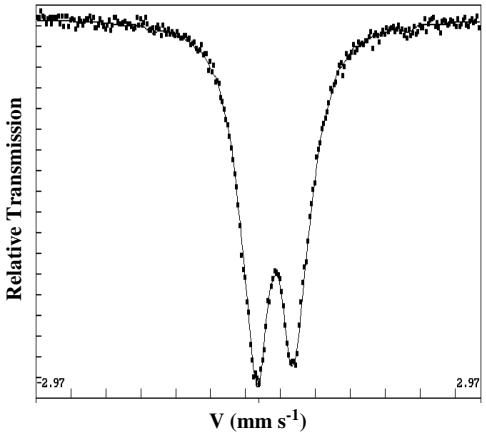


**Figure 7.** 300 K $^{57}$Fe Mössbauer spectrum of 6.6 nm $ZnFe_2O_4$ particles.

### *3.3. Mössbauer spectrometry*

The room temperature $^{57}$Fe Mössbauer spectra of $ZnFe_2O_4$ nanocrystals prepared in polyol appear to be quite similar. They consist of a quadrupolar doublet, in agreement with a superparamagnetic state, with broadened lines, as shown in figure 7, for the 6.6 nm particles. They can be reproduced using a large quadrupole splitting ($\Delta$) distribution linearly correlated with a narrow isomer shift ($\delta$) one. The $\delta$ range is characteristic of $Fe^{3+}$.

At 4.2 K, a magnetic ordering is indicated in the Mössbauer spectra for both samples. Indeed, the spectra for both 6.6 (figure 8(a)) and 14.8 nm (not shown) particles show a sextet typical of the magnetic hyperfine splitting of the iron ion, although the absorption lines for both spectra show considerable broadening. The Mössbauer spectrum of 6.6 nm particles can be well fitted with two sextets with Lorentzian lines, corresponding to tetrahedral and octahedral $Fe^{3+}$ contributions, according to the cation inversion previously established by EXAFS and XMCD measurements [14]. The refined values of the Mössbauer parameters are given in table 3. There is no evidence for the presence of the $Fe^{2+}$ charge state, which confirms the perfect stoichiometry of the two samples. It is therefore important to emphasize that numerous fitting models can be also proposed based on two narrow hyperfine field distributions, corresponding to tetrahedral and octahedral $Fe^{3+}$ sites with the same ratio. It would be thus necessary to estimate the hyperfine field distribution from the effective field distribution obtained from in-field Mössbauer spectra providing the distribution of canting angles be found. Such work is in progress.

At 10 K, in an external magnetic field of 6 T, applied parallel to the gamma-ray direction (figures 8(b) and (c)), the hyperfine structure reveals a splitting of the outermost lines. The first and the sixth lines of the spectra display a double-peaked structure contrasting with the single peak at these positions in zero field. Such a feature evidences the ferrimagnetic character of the magnetic ordering in these samples. Indeed, the hyperfine field is parallel to the applied field for the A site and antiparallel to the applied field for the B site, leading to shifted subspectra of the A and B sites. It is important to emphasize that the hyperfine field at $^{57}$Fe site is oriented antiparallel to its magnetization in the case of ionic oxides because of its large and negative value of the prevailing Fermi term. The hyperfine field parameters obtained from the fits are given in table 3. The fitted values of the degree of structure inversion, namely 25 and 18%

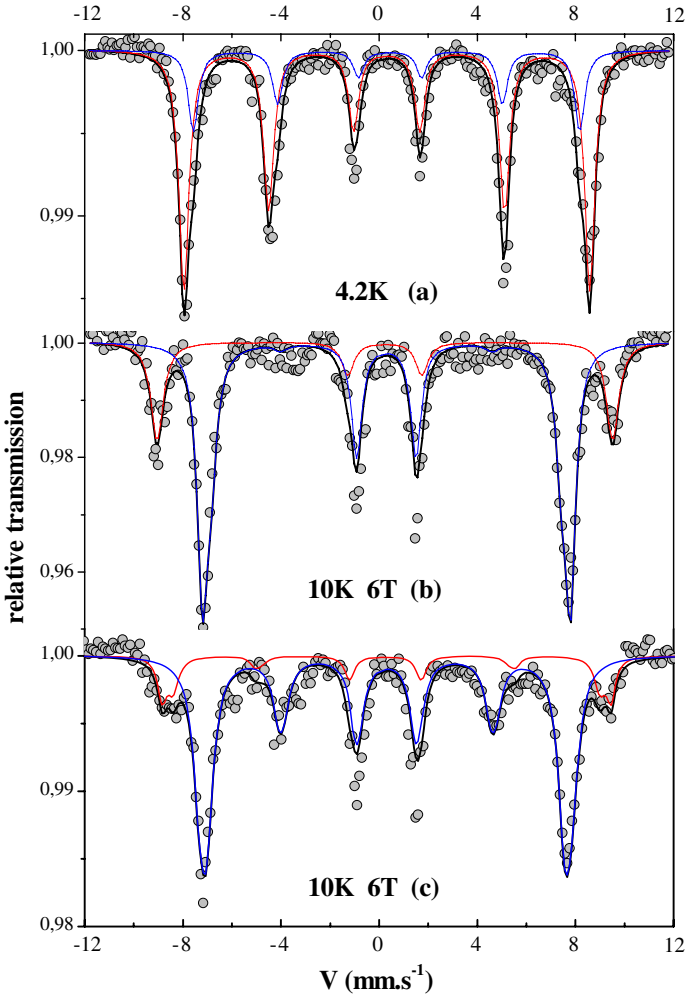


**Figure 8.** Zero-field (a) and 6 T field Mössbauer (b) spectra recorded at 4.2 K and at 10 K, respectively, for 6.6 nm $ZnFe_2O_4$ particles and a 6 T field Mössbauer spectrum (c) recorded at 10 K for 14.8 nm $ZnFe_2O_4$ particles.

**Table 3.** Fitted Mössbauer parameters for 6.6 and 14.8 nm $ZnFe_2O_4$ particles. Values of the isomer shift (IS) relative to that of $\alpha$-Fe at 300 K, the quadrupole shift ($2\varepsilon$), the hyperfine field $B_{hyf}$, the effective field $B_{eff}$, the average canting angle $\theta$ and the relative proportion of each $Fe^{3+}$ component.

| Size (nm) | Site | $B_{app}$ (T) | $\delta$ (mm $s^{-1}$) $\pm$ 0.01 | $2\varepsilon$ (mm $s^{-1}$) $\pm$ 0.01 | $B_{hyf}$ (T) $\pm$ 2 | $B_{eff}$ (T) $\pm$ 2 | $\theta$ (deg) $\pm$ 2 | Ratio (%) $\pm$ 1 |
|---|---|---|---|---|---|---|---|---|
| 6.6 | $Fe_A^{3+}$ | 0 (4.2 K) | 0.43 | 0.00 | 51.1 | — | — | 25 |
| | $Fe_B^{3+}$ | 0 (4.2 K) | 0.50 | 0.00 | 48.6 | — | — | 75 |
| | $Fe_A^{3+}$ | 6 (10 K) | 0.44 | 0.00 | 51.4 | 57.4 | 0 | 25 |
| | $Fe_B^{3+}$ | 6 (10 K) | 0.52 | 0.00 | 51.6 | 45.7 | 10 | 75 |
| 14.8 | $Fe_A^{3+}$ | 6 (10 K) | 0.41 | 0.00 | 50.9 | 55.7 | 35 | 18 |
| | $Fe_B^{3+}$ | 6 (10 K) | 0.44 | 0.00 | 50.6 | 45.7 | 38 | 82 |

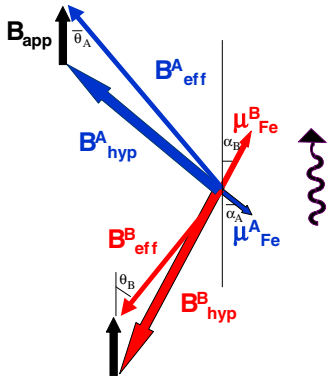


**Figure 9.** Schematic vector diagram of the hyperfine fields at A and B spinel sites in an applied field.

for the 6.6 and 14.8 nm particles, respectively, are in good agreement with those determined elsewhere by other techniques (EXAFS and XMCD) [14]. Hence, we will adopt these values, since they are more precise than EXAFS or XMCD determinations.

Close inspection of the in-field spectra of the 6.6 and 14.8 nm particles shows that the second and fifth lines have almost zero intensity for the first, and a non-vanishing intensity for the second. Usually, when these peaks are distinctly observed they evidence a canted structure for iron spins with respect to the applied field in both A and B sites. In the present case, local spin canting is only clearly apparent for the larger particles which exhibit the lower surface to volume ratio and the lesser degree of structure inversion, and this permits us to decide in favour of the existence, in this sample, of a canted Yafet–Kittel-like ferrimagnetic structure, as already suggested by DC magnetic measurements. In contrast, for the smaller particles, canting is less evident and we conclude in favour of a close to collinear Néel-like ferrimagnetic structure, the surface effects being rather weak.

The average canting angles (table 3) have been calculated from the ratio of the line intensities of $A_{2,5}$ to $A_{1,6}$. These values allow us to estimate the hyperfine field through the following relationship:

$$B_{\mathrm{hyf}}^2 = B_{\mathrm{eff}}^2 + B_{\mathrm{app}}^2 - 2B_{\mathrm{eff}}B_{\mathrm{app}}\cos(\theta) \tag{6}$$

where $B_{\mathrm{eff}}$ corresponds to the vectorial sum of the hyperfine field $B_{\mathrm{hyf}}$ and the applied field $B_{\mathrm{app}}$ (figure 9). The canting angles are found to decrease when the particle size decreases. This feature must be underlined, because it is completely different from that reported by the majority of authors for almost equivalent systems prepared by other routes. Indeed, Li *et al* found that $ZnFe_2O_4$ particles prepared by the sol–gel route with average diameters of 6 and 20 nm, and having almost the same degree of structure inversion, about 19%, exhibit a canting angle which increases when the particle size decreases [31, 32]. These experiments establish clearly that the measured canting angles are strongly affected by the spin glass-like surface contribution, which increases when the surface/volume ratio increases and then when the particle size decreases. They also found that particles prepared by different routes, as sol–gel and high energy ball milling, with roughly the same particle size, about 20 nm, and the same degree of structure inversion, about 20%, exhibit a canting angle which increases when the crystallinity of the particles decreases, showing that the canting angle is strongly affected by the structural disorder contribution which increases when the synthesis conditions, such as ball milling, favour structural defects.

In the present case, the observed variation of the canting angle with particle size decrease confirms that the results obtained from DC magnetic measurements (SQUID) and Mössbauer spectrometry are representative of the intrinsic magnetic properties of the partially inverted $ZnFe_2O_4$ spinel ferrite. The reduction of size effects such as the surface and/or core structural disorder are almost negligible, in agreement with the high crystallinity of both 6.6 and 14.8 nm polyol-prepared particles observed elsewhere by high resolution transmission electron microscopy (HRTEM) [14]. Moreover, it appears that when the concentration of magnetic ions in A sites is significantly higher than the percolation limit, a third magnetic model has to be considered in the description of the magnetic properties of partially inverted $ZnFe_2O_4$ spinel ferrite. For instance, for a concentration of 0.5, a close to collinear Néel-like ferrimagnetic ordering takes place.

## 4. Conclusion

$ZnFe_2O_4$ powders, with an average particle size of 6.6 and 14.8 nm, prepared by forced hydrolysis in polyol exhibit ferrimagnetic behaviour at low temperature, whereas the bulk material has long been known as antiferromagnetic with a transition temperature $T_N$ of about 10 K. The cationic distribution in the prepared $ZnFe_2O_4$ nanoparticles, affected by the crystal size, corresponds to a degree of inversion ranging from 25 to 18% when the size increases from 6.6 to 14.8 nm. These nanoparticles give rise to a large magnetization even at room temperature, with a saturation magnetization value which increases when the particle size decreases. Ferrimagnetic ordering is confirmed by the in-field low temperature Mössbauer study. The observed canting of Fe spin in both the A and B sites seems to depend on the particle size and consequently on the degree of structure inversion. It is almost zero for the 6.6 nm particles and higher for the 14.8 nm ones, suggesting the establishment at low temperature of a close to collinear Néel-like ferrimagnetic structure for the former and a canted Yafet–Kittel-like ferrimagnetic structure for the latter. Moreover, the high crystallinity of the polyol-prepared particles is not compatible with the occurrence of an important spin glass-like surface and/or core in these materials. Consequently, this work has demonstrated a close relationship between the observed magnetic properties of $ZnFe_2O_4$ nanoparticles and their local structure.

## References


[1] Smith S and Wijn H P J 1961 *Ferrites* (Amsterdam: Philips Library)
[2] Schiessl W, Potzel W, Karzel H, Steiner M, Kalvius G M, Martin A, Krause M K, Halevy I, Gal J, Shäfer W, Will G, Hillberg M and Wäppling R 1996 *Phys. Rev.* B **53** 9143
[3] Sato T, Haneda K, Seki M and Iijima T 1990 *Appl. Phys.* A **50** 13
[4] Anantharaman M R, Jagatheesan S, Malini K A, Sindhu S, Narayanasamy A, Chinnasamy C N, Jacobs J P, Reijne S, Seshan K, Smits R H H and Brongersma H H 1998 *J. Magn. Magn. Mater.* **189** 83
[5] Sidhu P S, Gilkes R J and Posner A M 1978 *J. Inorg. Nucl. Chem.* **40** 429
[6] Ueda M, Shimada S and Inagaki M 1993 *Trans. Mater. Soc. Japan* A **14** 23
[7] Oliver S A, Harris V G, Hamdeh H H and Ho J C 2000 *Appl. Phys. Lett.* **76** 2761
[8] Hamdeh H H, Ho J C, Oliver S A, Willey R J, Oliveri G and Busca G 1997 *J. Appl. Phys.* **81** 1851
[9] Hochepied J F, Bonville P and Pileni M P 2000 *J. Phys. Chem.* B **104** 905
[10] Pannaparayil T, Komamrneni S, Marande R and Zardaka M 1990 *J. Appl. Phys.* **67** 5509
[11] Andres-Verges M, Martinez M and Matijevic E 1993 *J. Mater. Res.* **8** 2916
[12] Goya G F and Rechenberg H R 1999 *J. Magn. Magn. Mater.* **203** 141
[13] Chinnasamy C N, Narayanasamy A, Ponpandian N, Chattopadhyay K, Guérault H and Greneche J M 2000 *J. Phys.: Condens. Matter* **12** 7795
[14] Ammar S, Jouini N, Fiévet F, Stephan O, Marhic C, Richard M, Villain F, Cartier C, Brice S and Sainctavit P 2004 *J. Non-Cryst. Solids* **245/246** 673
[15] Jeyadevan B, Tohji K and Nakatsuka K 1994 *J. Appl. Phys.* **76** 6325

[16] Kamiyama T, Haneda K, Sato T, Ikeda S and Asano H 1992 *Solid State Commun.* **81** 563
[17] Goya G F, Rechenberg H R, Chen M and Yelon W B 2000 *J. Appl. Phys.* **87** 8005
[18] Sato T, Haneda K, Seki M and Iijima T 1992 *Solid State Commun.* **7** 81
[19] Goya G F and Leite E R 2003 *J. Phys.: Condens. Matter* **15** 641
[20] Hubsch J, Gavoille G and Bolfa J 1978 *J. Appl. Phys.* **49** 1363
[21] Burghart F J, Potzel W, Kalvius G M, Schreier E, Grosse G, Noakes D, Schäfer R W, Martin A and Krausse M K 2000 *Physica* B **289/290** 286
[22] Kodama R H 1999 *J. Magn. Magn. Mater.* **200** 359
[23] Ammar S, Helfen A, Jouini N, Fiévet F, Villain F, Rosenman I, Danot M and Molinié P 2001 *J. Mater. Chem.* **10** 186
[24] Curuntu D, Remond Y, Chou N H, Jun M J, Caruntu G, He J, Goloverda G, O'Connor C and Kolesnichenko V 2002 *Inorg. Chem.* **41** 6137
[25] Chkaoundali S, Ammar S, Jouini N, Fiévet F, Richard M, Villain F, Greneche J M, Danot M and Molinié P 2004 *J. Phys.: Condens. Matter* **16** 4357
[26a] Tung L D, Kolesnichenko V, Caruntu G, Caruntu D, Remond Y, Golub V O, O'Connor C J and Spinu L 2002 *Physica* B **319** 116
[26b] Grasset F, Labhsetwar N D L, Park D C, Saito N, Haneda H, Cador O, Roisnel T, Mornet S, Duguet E, Portier J and Etourneau J 2002 *Langmuir* **18** 8209
[27a] Martin D H 1967 *Magnetism in Solids* (Cambridge, MA: MIT Press)
[27b] Zhang D, Klabunde K J, Sorensen C M and Hadjipanayis G C 1998 *Phys. Rev.* B **58** 14167
[28a] Chen J P, Sorensen C M, Klabunde K J, Hadjipanayis G C, Devlin E and Kostikas A 1996 *Phys. Rev.* B **54** 9288
[28b] Linderoth S, Balcells L, Laborta A, Tejada J, Hendriksen P V and Sethi S A 1993 *J. Magn. Magn. Mater.* **124** 269
[28c] Roy S, Dubenko I, Edorh D D and Ali N 2004 *J. Appl. Phys.* **96** 1202
[29] Gilleo M A 1960 *J. Phys. Chem. Solids* **13** 33
[30] Dutta P, Manivannan A, Seehra M S, Shah N and Huffman G P 2004 *Phys. Rev.* B **70** 174428
[31] Wang L, Zhou Q and Li F S 2004 *Phys. Status Solidi* b **241** 377
[32] Li F S, Wang L, Wang J B, Zhou Q G, Zhou X Z, Kunkel H P and Williams G 2004 *J. Magn. Magn. Mater.* **268** 332
[33] Bluncson C R, Thompson G K and Evans B J 1994 *Hyperfine Interact.* **90** 353
[34] Yu S H, Fujino T and Yoshimura M 2003 *J. Magn. Magn. Mater.* **256** 420
[35] Yafet Y and Kittel C 1952 *Phys. Rev.* **87** 290
[36] Evain M 1992 *Private Publication* (Nantes: Institut Jean Rouxel des Matériaux)
[37] Zheng M, Wu X C, Zou B S and Wang Y J 1998 *J. Magn. Magn. Mater.* **183** 152
[38] Dormann J L, Fiorani D and Yamani M E 1987 *Phys. Lett.* A **120** 95
[39] Makhlouf S A, Parker F T and Berkowitz A E 1997 *Phys. Rev.* B **55** R14717
[40] Chantrell R W, Walmsley N, Gore J and Marylin M 2000 *Phys. Rev.* B **64** 24410
[41] Charles S W and Popplewell J 1982 *Ferromagnetic Materials* (Amsterdam: North-Holland)
[42] Sepelak V, Steinike U, Uecker D C, Wissmann S and Becker K D 1998 *J. Solid State Chem.* **135** 52
[43] Druska P U, Steinike A and Sepelak V 1999 *J. Solid State Chem.* **146** 13